Article

Programmable and flexible wood-based origami electronics

Huashuo Ma[1,7], Chaozheng Liu[1,7], Zhi Yang[1], Shuai Wu[1], Yue Jiao[1], Xinhao Feng[2], Bo Xu [3], Rongxian Ou[4], Changtong Mei[1], Zhaoyang Xu[1], Jianxiong Lyu[1], Yanjun Xie [5] ✉ & Qiliang Fu [1,6] ✉

Natural polymer substrates are gaining attention as substitutes for plastic substrates in electronics, aiming to combine high performance, intricate shape deformation, and environmental sustainability. Herein, natural wood veneer is converted into a transparent wood film (TWF) substrate. The combination of 3D printing and origami technique is established to create programmable wood-based origami electronics, which exhibit superior flexibility with high tensile strength (393 MPa) due to the highly aligned cellulose fibers and the formation of numerous intermolecular hydrogen bonds between them. Moreover, the flexible TWF electronics exhibit editable multiplexed configurations and maintain stable conductivity. This is attributed to the strong adhesion between the cellulose-based ink and TWF substrate by non-covalent bonds. Benefiting from its anisotropic structure, the programmability of TWF electronics is achieved through sequentially folding into predesigned shapes. This design not only promotes environmental sustainability but also introduces its customizable shapes with potential applications in sensors, microfluidics, and wearable electronics.

Emerging high-tech (e.g., smart cell phones, computers, and displays) progress has led to increasing consumption of electronic products that are made from non-renewable and non-biodegradable resources[1,2]. To date, flexible electronic devices have attracted extensive attention in broad applications, such as sensors[3–5], wearable devices[6–9], e-skins[2,10–13], electronic circuits[14,15], microfluidics[16,17] and soft robotics[18]. This is due to their customized and portable size, multifunction, and excellent biocompatibility. However, the increase of e-waste has led to severe environmental pollution and serious energy consumption problems, which have brought great challenges to the development of flexible electronic devices[19]. Therefore, the evolution of future flexible electronics focuses on innovation towards environmentally friendly and sustainable devices, which are highly desirable for the next generation of flexible electronics[20].

Wood-based cellulose and its natural derivatives are sustainable carbohydrate polymers, which are widely constructed via bottom-up and top-down strategies[21–25]. They can be used to produce advanced functional electronics with high transparency, excellent mechanical properties, and low thermal conductivity in various applications, such as optoelectronics[26], smart displays[27], electroluminescent devices[28] and sensors[29,30]. The bottom-up approach starts from low-dimensional cellulose building blocks assembling to 2D or 3D nanomaterials that couple with conductive materials to obtain strong and flexible electronic devices[31–34]. While an alternative top-down strategy based on the bulk wood or veneer has enabled it the direct conversion into a

[1]Co-Innovation Center of Efficient Processing and Utilization of Forest Resources, College of Materials Science and Engineering, Nanjing Forestry University, Nanjing, PR China. [2]College of Furnishings and Industrial Design, Nanjing Forestry University, Nanjing, PR China. [3]MIIT Key Laboratory of Advanced Display Materials and Devices, School of Materials Science and Engineering, Nanjing University of Science and Technology, Nanjing, PR China. [4]Institute of Biomass Engineering, South China Agricultural University, Guangzhou, PR China. [5]Engineering and Engineering Research Center of Advanced Wooden Materials, College of Materials Science and Engineering, Northeast Forestry University, Harbin, PR China. [6]Scion, Te Papa Tipu Innovation Park, Rotorua, New Zealand. [7]These authors contributed equally: Huashuo Ma, Chaozheng Liu. ✉e-mail: yxie@nefu.edu.cn; qiliang.fu@njfu.edu.cn

substrate for the development of wood-based functional electronics[35,36]. Wood nanotechnologies have been achieved through the nano-control of the microstructure, composition and porosity, enabling high performance electronics with excellent mechanical and optical properties, and flexibility[37,38]. However, these wood-based electronics are constrained in their ability to undergo complex shape deformation, hindering their applications, in scenarios that demand custom sizes, foldable structures, editable shapes, and smart deformations.

Reconfiguration design enables the proposed material to be reconfigured after fabrication, endowing it with additional properties or application requirements[19,39,40], for example 3D printing and folding design. For cellulose-based substrates, control of their shape deformations are typically stimulated by such things as optics, heat, humidity-sensitivity, and electrical and magnetic responses. While origami-inspired technology is a paper-based folding art that transforms the 2D paper sheets into 3D structures with arbitrarily shape-editable features[41–44]. Pencil-on-paper is an attractive approach to achieve high-fidelity detection for a range of vital biophysical and biochemical signals from human bodies[45–47]. Yet, the conductive durability of the pencil-on-paper based electronics could be influenced by folding and deformation, as the carbon black is physically attached on paper substrates. Thanks to the rapid development of computer technology, various complexly patterned electronics can be designed by computer programs and 3D printing techniques, as well as enabling the conductive ink to be strongly attached to flexible electronics[48]. The typical gel ink made from the cellulose nanofibers (CNF) was chosen due to its strong adhesion and intricate network, as well as its adjustable rheological characteristics[49,50]. This integration has significantly spurred the development of origami crease designs for programmable devices, which are aimed at applying in soft robotics and grippers, deformable circuits, expandable stents, and smart actuators[41]. As far as we know, previous studies have been reported focusing on origami crease soft elastomers, stretch polymers, liquid crystals, and isotropic structured paper substrates[51–53]. However, there are few studies documenting flexible origami electronics based on thin wood films. Additionally, developing wood-based electronic devices with shape programmability and editability poses a significant challenge.

Herein, an editable and flexible wood origami electronic device is developed from the combination of a transparent wood film (TWF) substrate and cellulose-based conductive ink (Fig. 1). Lignin and partial hemicellulose are removed from natural wood cell walls, from which the honeycomb structure of wood is intensively collapsed and stacked with numerous exposed cellulose fiber bundles (Fig. 1a). This resulted in a densified and thin TWF substrate that can be printed with conductive ink to achieve wood-based electronics (Fig. 1b). The conductive ink consists of 2,2,6,6-tetramethylpiperidine-1-oxyl (TEMPO) oxidized cellulose nanofibrils (TOCNFs) and multi-walled carbon nanotubes (CNT) with favorable adhesion performance. The resulting wood-based electronics showed favorable mechanical properties and flexibility due to the highly aligned CNF in the substrate and the formation of hydrogen bonding between TWF and printed ink. Moreover, the origami-inspired design allowed for sequential folding into predesigned shapes for adapting to different application scenarios (Fig. 1c). The programmable configuration and stable electronic conductivity of the wood-based origami device were further evaluated. Furthermore, wood-based flexible origami electronic circuits exhibited favorable mechano-electronic sensing performance, which was demonstrated using a human motion sensor as a proof-of-concept (Fig. 1d). Coupling with the anisotropic microstructure of the TWF, the wood-based origami electronics offer potential as a sustainable and practical alternative (Fig. 1c).

Results

Morphology and physical performance of treated porous wood

Wood is a natural composite material that possesses a unique hierarchical structure, porosity, and multiple layers of cell walls, which are made up of three main components (lignin, hemicellulose, and cellulose) and other extractives. Cellulose microfibrils form the skeletons of the cell walls in the form of molecular chains aggregated into well-arranged microfibrillar bundles providing the mechanical support, while hemicellulose and lignin reinforce the cell wall making it a relatively rigid material (Fig. 2a). Natural balsa wood veneers with honeycomb-like structure show yellowish color because of the presence of chromophores and lignin (Supplementary Figs. 1 and 2), which are fluorescent and uniformly distributed in the cell wall of natural wood (Supplementary Fig. 3a). After the delignification process, most of the lignin (a relative value of 92.1 %) was removed from cell walls while preserving the honeycomb structure (Fig. 2c). The confocal fluorescent images of original wood (OW) and delignified wood (DW) further confirmed the lignin removal from cell walls (Supplementary Figs. 3 and 4). This resulted in the generation of microscale pores between cell walls of the DW sample (Fig. 2b and Supplementary Fig. 5)[54]. The DW appeared white due to the removal of chromophores (Supplementary Fig. 1 center). However, more than 90% hemicellulose remained in the DW sample due to the mild delignification, maintaining the relative cell wall rigidity.

Further alkali treatment (1 mol L^{-1} NaOH) was applied to swell and soften the delignified cell walls, this process is beneficial to increase density and transparency. More than half of the hemicellulose (58.3%, relative value) was hydrolyzed and removed from the porous wood (PW) sample (Fig. 2c), which enabled the creation of additional micro and nanoscale porosity in the secondary cell wall and corner with a specific surface area of 46.9 m^2 g^{-1} for the super critical dried PW sample (Supplementary Fig. 2b, 5). This value is much higher than the values of OW (1.1 m^2 g^{-1}) and DW (17.8 m^2 g^{-1}). Interestingly, after chemical treatment, most of cellulose was preserved both in the DW and PW samples (Fig. 2c). The absorption peaks at 3340 cm^{-1} and 1035 cm^{-1} of Fourier transform infrared spectroscopy spectra (FTIR) are assigned to the hydroxyl groups and C-O stretching of the cellulose (Supplementary Fig. 6), these signals were present in all samples indicating the composition of cellulose (Fig. 2c). After delignification and hydrolysis treatments, the swollen and softened cell walls were subjected to the densification and dehydration resulting in a dense and thin TWF around 50 ± 10 μm thickness (Fig. 2d). The collapsed cell walls were intensely stacked with a layered structure that exposed cellulose fibril bundles as shown from the cross-sectional SEM image (Fig. 2d). Moreover, the surface observations of TWF sample showed the full removal of microscale lumen spaces while maintaining the original arrangement of cell walls (Fig. 2e).

The dense and thin TWF material, characterized by its anisotropic structure, has the potential to exhibit excellent properties including optical and mechanical attributes[55]. As expected, the densification step completely removed air-containing micro- and nanopores from the TWF substrate, which resulted in a condensed cell wall with a refractive index of approximately 1.53 and showed a high transmittance of 78% and optical haze of 88% at the wavelength of 550 nm (Fig. 2f). The optical transmittance decreased with increasing the thickness of TWF due to the light scattering (Supplementary Fig. 7). More importantly, the Young's modulus and tensile strength of TWF in the longitudinal direction are 43.68 GPa and 393.8 MPa, which are 5–20 times higher than those of the OW, DW, printer paper, and polyethylene terephthalate (PET) substrates (Fig. 2g, and Supplementary Fig. 8). These values are comparable to most cellulose paper-based substrates, non-natural polymers, and petroleum-based plastic matrixes (Supplementary Table 1). This is mainly ascribed to the highly aligned cellulose in the fiber longitudinal direction of TWF (Fig. 2e, right). It is further confirmed by the 2D wide-angle X-ray diffraction (WAXS) result
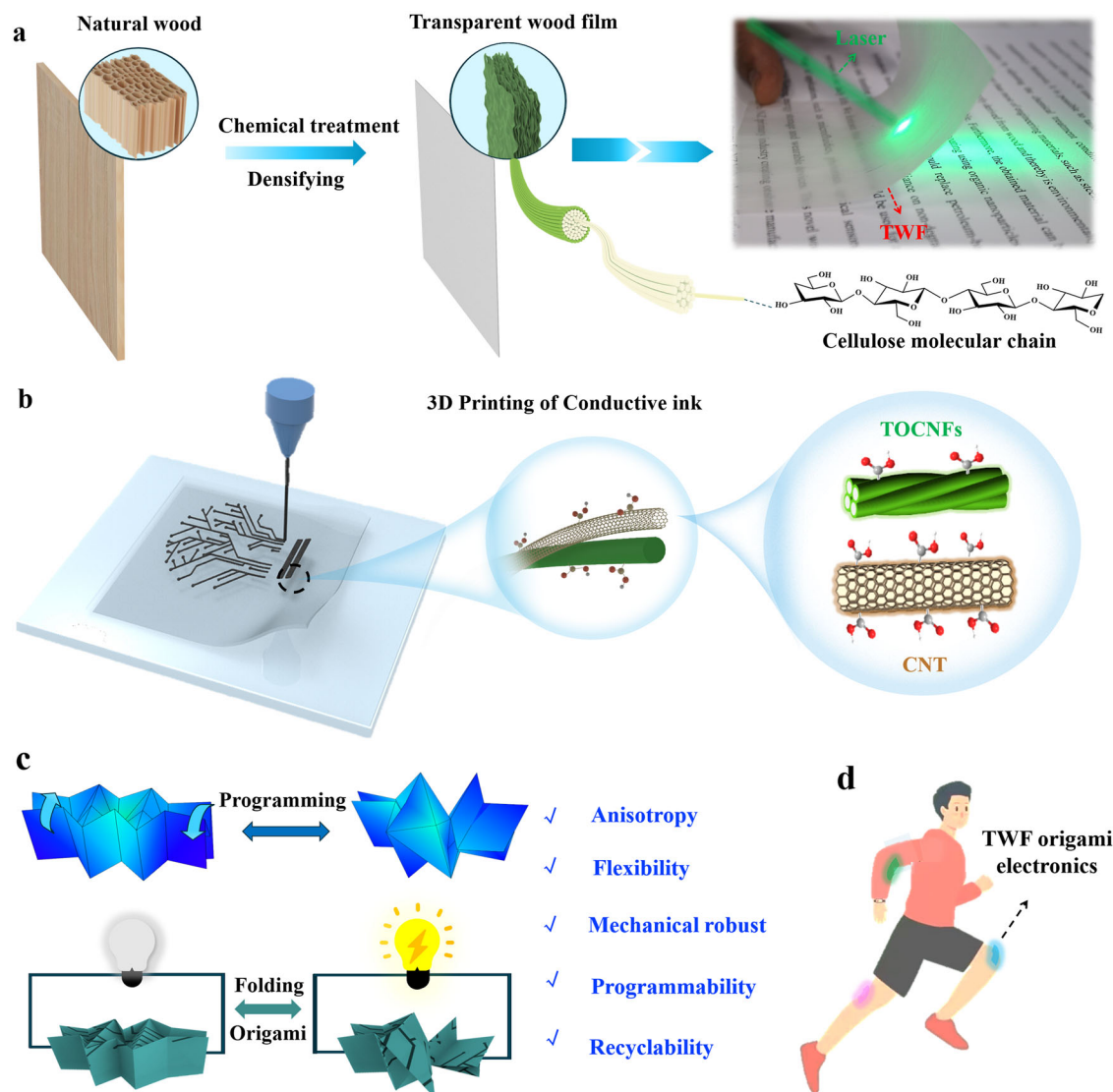
Fig. 1 | Schematic illustration of the flexible wood-based origami electronics. a The process of making TWF. **b** Preparation of a wood-based electronic device by 3D-printing cellulose-based conductive ink on a TWF surface. **c** The schematic illustration of wood-based origami electronic products with favorable shape programmability and stable conductivity under reversible folding/unfolding deformation. The advantages of TWF origami electronics are highlighted including anisotropy, favorable flexibility, mechanical robust, programmability and recyclability. **d** The potential application of TWF origami electrons in human motion sensors.

(Fig. 2h). The strong arcing diffraction spots are observed from 2D WAXS pattern of TWF corresponding to the cellulose crystal planes (200) and (110) (Fig. 2h, i), which suggests that the cellulose fibers were preferentially aligned in the direction of tree growth (Fig. 2e). A similar 2D WAXS pattern result was obtained from OW sample (Supplementary Fig. 9). In contrast, the scattering diffractogram of the isotropic copy paper presents a circle-like pattern (Supplementary Fig. 10). The sharp peak of the azimuthal integral of the (200) scattering plane for TWF indicates to a high orientation degree of cellulose fibers (orientation index = 0.88) (Fig. 2j)[29]. Moreover, the mechanical improvement of the TWF is also attributed to the formation of hydrogen bonding between the cellulose fibers in the fully collapsed wood cells[38]. The position of TWF shows in the Ashby chart of specific modulus versus specific strength among various materials demonstrating superior strength yet with a lightweight characteristic (Supplementary Fig. 11). Furthermore, the TWF sample exhibited favorable flexibility and underwent diverse deformations without cracking (e.g., rolling and knotting) (Supplementary Fig. 12), as well as excellent folding endurance and was able to fold more than 8000 times (Supplementary Fig. 13). This value is close to those of printer paper and PET substrates and cannot be achieved in natural and delignified wood (Supplementary Fig. 14). This inherent flexibility and mechanical performance support the TWF substrate as a suitable candidate for flexible electronics.

Preparation and electrical conductivity of flexible wood-based electronics

Direct ink writing (DIW) technology has rapidly developed and been proven to be an effective method for manufacturing intelligent and flexible cellulose-based electronics[56,57]. In this study, the conductive gel-like ink was prepared by combination of TEMPO oxidized cellulose nanofibers (TOCNFs) and CNT (Supplementary Fig. 15a), which was further developed from our previous study[58]. The rheological properties of CNT/TOCNFs conductive inks were characterized as displayed in Supplementary Fig. 16. The steady-state viscosities of CNT/TOCNFs inks with 2%, 4%, 6%, and 8% concentrations at a shear rate of $10^{-1}s^{-1}$ were 13.2, 20.1, 32.9 and 40.5 kPa s^{-1} (Supplementary Fig. 16), respectively. Conductive ink at a concentration of 4 % was selected for
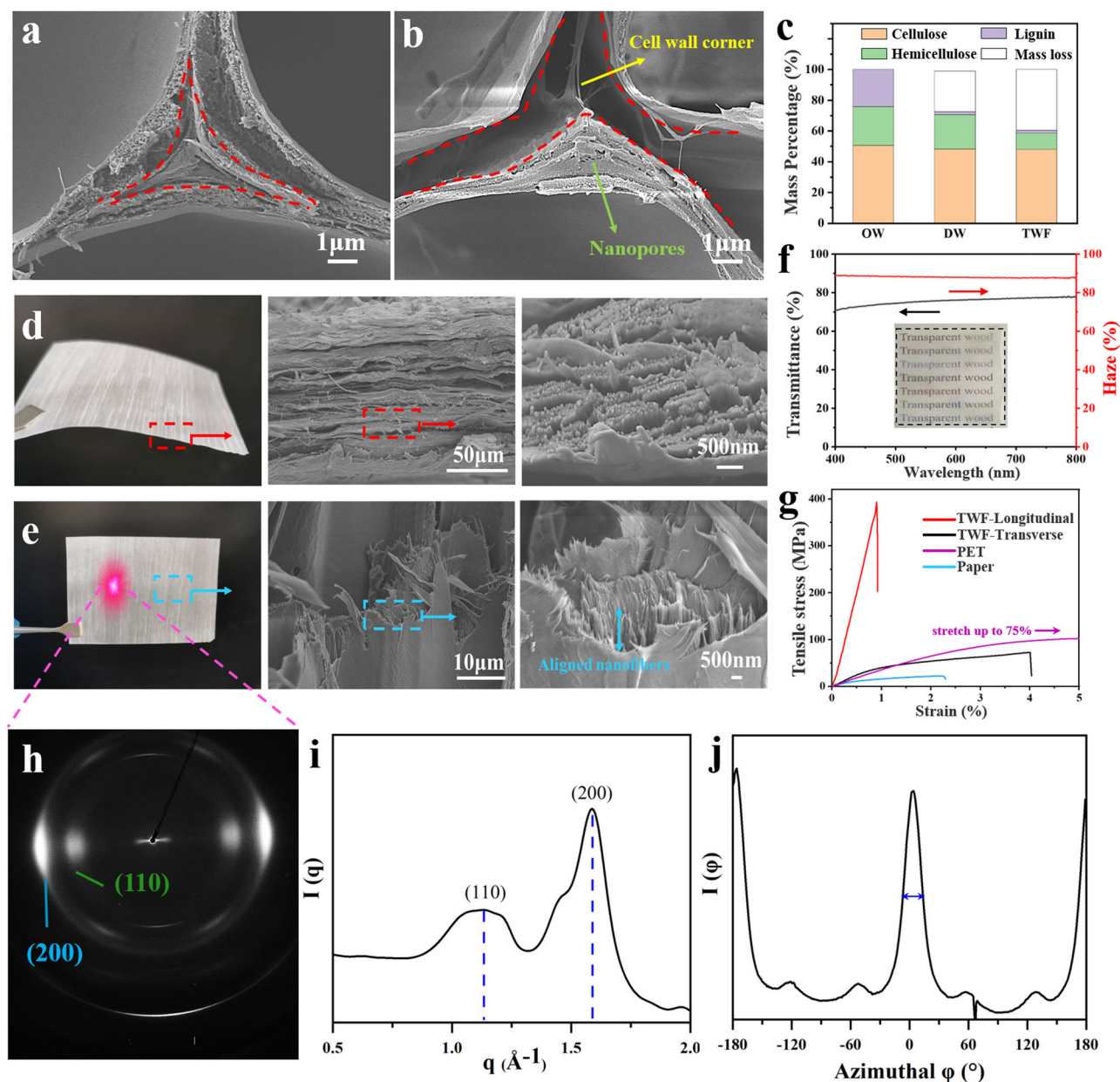
Fig. 2 | The morphological and structural characterizations of OW, PW and TWF. a, b Morphologies of OW and PW. **c** The chemical compositions of OW, PW, and TWF. **d, e** Photographs and SEM images of TWF shown in cross-section and surface. **f** Total transmittance and optical haze of TWF. **g** Typical stress-strain curves of TWF (both in longitudinal and transverse directions), PET and printer paper. **h** X-ray synchrotron WAXS pattern of TWF. **i** Radial integration of the diffractogram shown in (**h**). **j** Azimuthal integration of the (200) scattering plane of the diffractogram shown in (**h**).

printing due to favorable shape retention with continuous structure filament (Supplementary Fig. 15b). Moreover, the conductive inks show a typical shear-thinning behavior enabling the ink to flow uniformly, printing with an excellent shape fidelity (Supplementary Fig. 17)[50]. The prepared ink was printed onto the surface of TWF using the DIW technique showing excellent adhesion stability, which is mainly due to the formation of hydrogen bonding and van der Waals forces between the CNT/TOCNFs ink and the surface of TWF[59,60], as schematically shown in Fig. 3a[61].

The suitable substrates for the flexible electronics generally provide excellent interface adhesion, low surface roughness and thermal expansion index, and favorable mechanical properties[62]. The exceptional adhesion stability of the as-prepared ink enables the printing of diverse patterns and circuits on TWF surfaces (Fig. 3b). The micro-patterned circuits extend beyond simple straight lines to encompass

more intricate features suitable for adaptable electronics on the skin, such as the bulb and tree-like configurations (Supplementary Fig. 17). The appearance profile of the TWF substrate presented a surface roughness of about ± 100 nm as shown in the atomic force microscope (AFM) image (Fig. 3c). The printed layer around $1\,\mu m$ thickness was measured by SEM imaging (Supplementary Fig. 18a), where the printed TWF substrate resulted in an overall smooth surface as observed from the AFM image (Fig. 3d). The top-view SEM image of the printed TWF showed a distinct edge between the coated and un-coated area (Fig. 3e, left). While CNT/TOCNFs inks were randomly distributed and formed a densely packed network layer (Fig. 3e), where the tube-like CNT/TOCNF fibers were uniformly entangled and overlapped on the surface of the printed TWF electronics (Supplementary Fig. 18b). A sellotape peel-off experiment was further used to assess the adhesion between the ink and the substrate (Supplementary Fig. 19). After 15 cycles of the
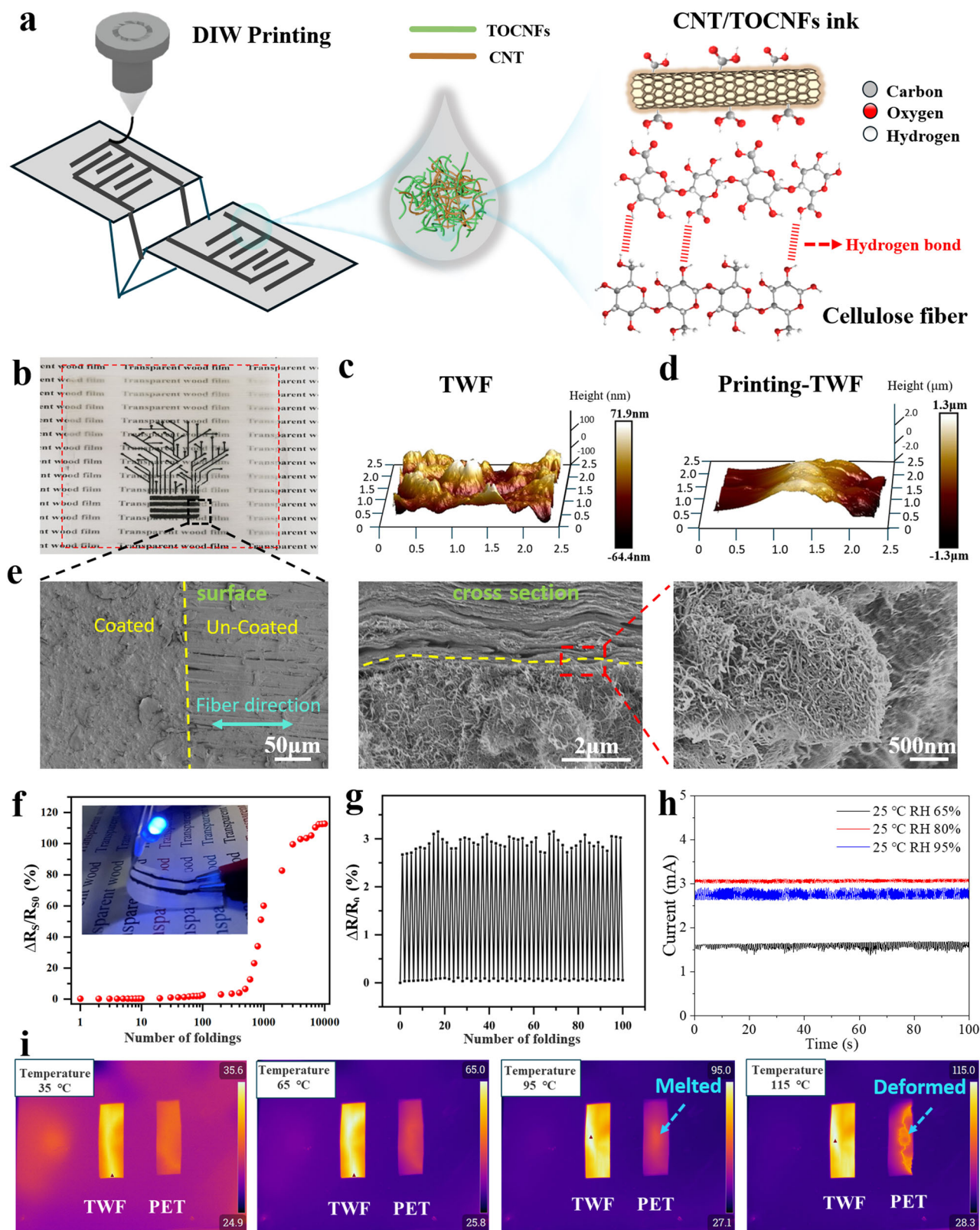
Fig. 3 | Schematic preparation of cellulose-based CNT/TOCNFs conductive ink and the TWF flexible electronics. a Schematic illustration of CNT/TOCNFs conductive ink and direct ink writing on the TWF surface. **b** Digital images of conductive ink printed on the surface of TWF. **c**, **d** Surface profile AFM images of TWF with and without printed with ink, respectively. **e** SEM morphologies of conduction ink on flexible electronic circuit observed from surface and cross-section, respectively. **f** Normalized sheet resistance variation of the TWF flexible circuit *versus* the number of folding−unfolding (180°) cycles. An inserted photograph of the TWF flexible circuit powering a LED. **g** Normalized relative resistance variation as a function of the number of foldings (90°). **h** The conductivity of the TWF electronics was measured at different relative humidity (RH) conditions. **i** The thermal infrared images of TWF and PET substrates heated at different temperatures (a range of 35−115 °C).

peeling test, the printed ink on TWF showed only minor peel-off while maintaining the integrity of the ink pattern, indicating a strong adhesion with the TWF substrate. However, the printed ink displayed detachment from a printer paper substrate in the 8th cycle of the test and increasing relative resistance ratio (Supplementary Fig. 19). This may be ascribed to the additives (i.e., starch, alum and CaO) in the printer paper. A further physical scraping study confirmed that TWF electronics possess favorable adhesion and a stable conductivity compared to those of printer paper and PET substrates (Supplementary Fig. 20).

The inter-connected CNT/TOCNFs networks are beneficial to transport electrons between them with a favorable conductivity. An average electrical conductivity of 0.24 S cm^{-1} was measured for the TWF electronic, which can active a blue light-emitting diode when it was bent (Fig. 3f). In addition, a stable resistance of the flexible TWF circuit is shown under the tensile, suggesting good adhesion between the TWF substrate and CNT/TOCNFs layer (Supplementary Fig. 21). To evaluate the folding endurance of the printed flexible TWF circuit, the electric conductive performance under cyclic folding/unfolding was investigated. The relative sheet resistance of the flexible circuit was almost unchanged within 500 folding/unfolding cyclic tests (Fig. 3f). The resistance change of the circuit during bending is also around 3%, indicating its conductive stability due to the strong combination of hydrogen bonding and van der Waals forces between the CNT/TOCNFs layer and TWF substrate (Fig. 3g)[63]. Yet, after 500 folding/unfolding cyclic tests, the resistance change ratio increased significantly, which may be attributed to the disruption of the structure between the conductive ink and the TWF substrate. The morphology of TWF and conductive ink at different folding stages was carefully examined. After 500-cycle test, a cracking line was generated on the surface of the printed ink layer (Supplementary Fig. 22). While a crease line can be observed from the surface of TWF substrate without any cracking or damage (Supplementary Fig. 23). The consistent conductive performance through repeated mechanical deformation demonstrates the potential for integration of this TWF circuit into advanced flexible electronic devices. Moreover, the conductivities of TWF electronics showed stable currents at relative humidity (RH) conditions of 65%, 80% and 95% (Fig. 3h), respectively. The current value of TWF electronics at high RH (80% and 95%) is higher than that of low RH (65 %) due to the water molecules facilitating the electrons transport along the conductive ink. Furthermore, TWF demonstrated a favorable thermal tolerance performance compared to the PET substrate (Fig. 3i). The PET film was melted at 95 °C following by a deformation at the temperature of 115 °C. While the TWF film presented thermal and dimensional stabilities under a temperature range of 35–115 °C because of the low thermal expansion coefficient and conductivity of cellulose fibrils (Supplementary Fig. 24)[64,65]. Although the output current of TWF electronics at high temperature (115 °C) was the lowest due to the moisture evaporation, the current signals were stable under 35–95 °C conditions indicating an excellent thermal tolerance of TWF electronics (Supplementary Fig. 25).

## Programmable design of the flexible TWF origami electronics

Programmable design is established for folding and unfolding to transform a flat structure into an origami feature with inherent shape editability and deformation. Due to its excellent adaptability and shape reversibility, it is widely used to construct 3D structures[66–68]. An origami structure is demonstrated and designed to achieve freedom in two dimensions, allowing for transformations along two different dimensions; for instance, one might be folding along a transverse direction while another one could be along a longitudinal direction. The 2D freedom origami offers shape editability and flexibility through the TWF substrate design capabilities[69].

The natural anisotropy of TWF, retained from its wood structure, serves as an enticing feature for designing origami electronic products.

For example, anisotropy affects the direction dependence of TWF during folding. This characteristic facilitated precise folding into various configurations of the origami structure without causing cracks or damage to the electronics. The prediction of the performance of origami structure in different folding angles and directions through computer modeling and numerical simulation can be used to optimize the design and achieve specific functional requirements. Herein, origami crease patterns were predesigned as shown in the Fig. 4a, which included different types of creases, such as mountain creases (red), valley creases (blue), and border creases (black) (Fig. 4a, left). According to the design requirements, flexible creases (purple) can be adjusted within a certain range and modeled as an arbitrary linkage position or angle. Moreover, the origami crease patterns are predesigned by computer programs that allow various shapes deformability and dynamism, which is especially important when creating origami features with dynamic structures or variable shapes[70]. Faceted folds (green) are folds that attempt to remain flat (0° fold angle) when the pattern is folded (Fig. 4a, center). The deformations of the TWF substructure are in the direction of the fibers leading to symmetrical reconfiguration from side to side (Fig. 4a, right). The center creases in the TWF substrate can be programmed to fold at 90° and 45° enabling the transformation of two different macroscopic morphologies, which are reversible and switchable by applying programmable torque transformations.

To understand and predict the mechanical behavior of origami structures, a finite element method (FEM) analog simulation is performed through a strain visualization study (Supplementary Fig. 26 and Supplementary Table 2)[71]. The FEM employs realistic material models and higher-order elements to explore the structural characteristics of origami in fully or partially folded states. The stress distribution from a flat TWF substrate to the pre-designed origami configuration was subjected to theoretical and numerical analysis (Fig. 4b and Supplementary Figs. 27–29). The strain during the folding process was converted to RGB colors on the blue (no strain) to red (high strain) spectrum resulting in the 3D model for visualization. As shown in Fig. 4b, the strain from the initial state to the intermediate state is presented with the maximum principal strain of the deformed structure being less than 5%. The deformation of the TWF substrate occurred at the elastic region during the folding process enabling the reversible transformation of its configuration (Supplementary Fig. 27). The elastic deformations in both longitudinal and transverse directions are anisotropic due to the inherent anisotropic nature of wood (Fig. 4c). A steeper slope in the longitudinal curve indicates that the device is more resistant to this deformation (Fig. 4c). The changes in the geometry by telescopic and torsional folding at different states were further simulated (Supplementary Figs. 28 and 29). The shape and structure of the TWF substrate can be manipulated by manually applying force in the loading direction. The stress-displacement and the stress-folding percentage curves suggest that the telescopic folding presents an overall smoother pattern in comparison to the torsional folding, indicating more predictable and uniform transformation behavior (Supplementary Fig. 30). The specific simulation of tailoring geometry and strain visualization is detailed in Supplementary Movies 1, 2.

The programmable shape and editable capability enable the flexible wood-based origami electronic sensor to monitor various human body motions. A patterned CNT/TOCNFs wood-based origami sensor that can be switched on or off in different folding states was designed (Fig. 4d, e). The sensor was disconnected when it was in original state. However, when it was rotated at 90°, the 3D-printed conductive pattern was successfully connected and powered the LED bulb (Fig. 4d). This is a reversible on/off process that depends on the deformation of wood-based origami sensor. Moreover, various geometries of TWF substrate and printing patterns can be made by combining the origami and DIW technologies (Supplementary Fig. 31). The
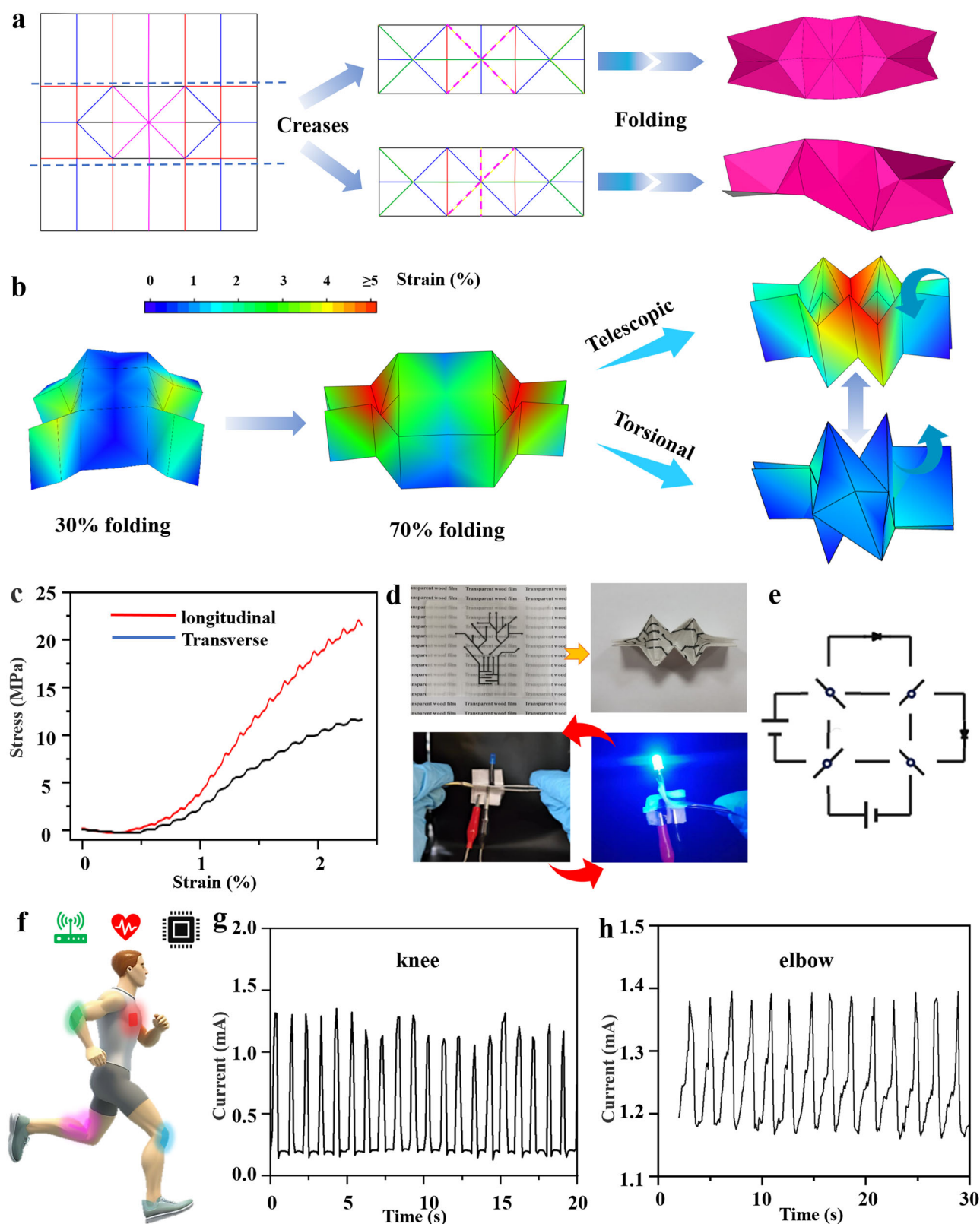
Fig. 4 | The simulation and potential application of programmable and flexible wood-based origami electronics. a Schematic diagram of creases. **b** FEM visualization of the wood-based origami electronic under different folding states. Blue and red color represent 0% and ≥5% strain, respectively. **c** Curves of stress *versus* strain generated from the FEM prediction. **d** Digital images of programmable and flexible wood-based origami electronics. **e** Schematic diagram of the circuit. **f** Potential application of wood-based origami electrons for the smart sensor. Curves of output current for monitoring movement of the knee (**g**) and elbow (**h**), respectively.

wood-based origami electronics were demonstrated and the application of a smart wearable sensor for monitoring human movements as a proof-of-concept, which was adapted to the human body for collecting electrical signals that fluctuated with motion (Fig. 4f). For real-time monitoring of various human movements, the smart sensor was attached to the knee and elbow joints (Fig. 4f, and Supplementary Fig. 32). When the knee or elbow repeatedly bent to a certain angle resulting in folding-unfolding of the TWF origami electronics, which simultaneously recorded output currents with relatively stable signals (Fig. 4g, h). Different rates and amplitudes of body movements generated stepwise signals in the current. For example, increased relative resistance was recorded when running speeds increased from 5 to 20 km h^{-1} (Supplementary Fig. 33). Furthermore, the different extents of current change in the longitudinal and transverse directions are ascribed to the anisotropic structure of TWF substrate (Supplementary Figs. 36 and 37). This may be associated to the stretching of the covalent bonds (glycosidic bonds) in the longitudinal direction in comparison to the non-covalent bonds (hydrogen bonds and van de Waal forces) in the transverse direction. Current changes of the sensor were detected due to manually applied finger pressure (Supplementary Fig. 36). Finally, we proposed the recycling processes for electronic products made from TWF substrates (Supplementary Fig. 37). The recycled wood-based membrane demonstrated favorable mechanical stability even after 10 cycles of recycling (Supplementary Fig. 38), which is comparable to isotropic structure of cellulose nanopaper. Increasing the recyclability of materials can increase the total service life and sustainability, as well as reducing electronic waste and carbon footprint. Moreover, a closed-loop recyclable manufacturing process is proposed to produce final products that could be explored as alternatives of fossil-based plastics in green packaging materials and electronics (Supplementary Fig. 37). These encouraging results suggest that programmable and flexible wood-based origami electronics have great potential in various applications, such as wearable smart devices, soft robotics, and intelligent sensors.

Discussion

In summary, programmable and flexible wood-based origami electronics were developed for advanced and sustainable electronic devices. By harnessing advancements in wood nanotechnology, the delignified and softened porous wood was densified into a thin and transparent wood-based substrate that can be manipulated into different shapes and printed with conductive CNT/TOCNFs ink for smart wood-based origami electronics, which possesses excellent tensile strength due to the preservation the original cell wall architecture with highly aligned cellulose fibers. Moreover, the cellulose-based conductive ink was printed on to the TWF substrate and had strong interface adhesion owning to the formation of hydrogen bonds and van der Waals forces. The flexible wood-based electronics showed a favorable and stable conductivity with no limit to various deformations (e.g., bending, folding and rolling) thanks to the homogeneous inter-connected CNTs with electron transportation. The origami-inspired design and DIW technologies enable to the creation of electronic devices that are not only flexible but also shape-editable with any desired architectures, extending their potential applications for more complex and dynamic scenarios. The implementation of flexible wood-based origami electronic sensor devices demonstrates the detection of stable electrical signals in wearable and motion monitoring. Furthermore, the mechanical property of the recycle substrates are comparable to the randomly constructed cellulose-based materials even after multiple recycling processes indicating a superior recyclability. Coupling with wood nanotechnology, the highlight of this study is to propose an approach for designing flexible wood-based origami electronics from the anisotropic structure of natural wood, which is challenging to overcome in some traditional materials, for example printer papers and plastics. With a view to future work, we believe that the proposed approach provides a new solution for the designing wood-based smart and flexible electronics that could extend the potential applications in sensors, wearables, e-skins, and soft robotics.

Methods

Materials and chemicals

The Balsa wood veneers (*Ochroma pyramidale*) with a density of 0.15 g cm^{-3} had dimensions of $80 \times 80 \times 1$ mm^3 (longitudinal× radial× tangential). Sodium chlorite (80%, NaClO$_2$), sodium hydroxide (98%, NaOH), 2,2,6,6-tetramethylpiperidine-1-oxyl (TEMPO) and sodium bromide (NaBr) were supplied by Aladdin Industrial Co., Ltd (Shanghai, China). Acetic acid (CH$_3$COOH), sodium acetate (CH$_3$COONa), multi-walled carbon nanotube (CNT) were purchased from Nanjing Chemical Reagent Co., Ltd. (Nanjing, China). Poly (ether sulfone) (PES, 30 nm pore size and 150 mm diameter) filter membrane was provided by Sterli Tech Ltd., (Auburn, USA). Polyethylene terephthalate (PET) film was supplied from Convex Innovative Packaging (New Zealand).

Delignification process and fabrication of Transparent Wood Film

The balsa wood veneers were delignified by 1 wt% of NaClO$_2$ in acetate buffer solution (pH ≈ 4.6) at 80 °C for 6 h, following by softening of the cell wall and removal of hemicellulose using 1 mol L^{-1} NaOH solution at room temperature for 3–6 h. The delignified and softened samples were completely washed with deionized water to remove extra chemicals. This process was repeated three times. The wet treated wood veneers were placed between two PES membranes and filter paper and densified (≈3–5 kg) at room temperature and dried for 24–48 h to achieve the thin and dense TWF substrates (50 ± 20 μm in thickness, and 1.3 g cm^{-3} in density). These fabrication processes refer to our previous study[29].

Preparation of CNT/TOCNFs Conductive Ink

The preparation of TOCNFs was developed from our previous reported literature[58]. Specifically, taking a concentration of 4 wt% CNT/TOCNFs solution as an example. Approximately 1 g of cellulose fibers were dissolved in 150 mL of deionized water, followed by the addition of 0.016 g of TEMPO and 0.1 g of NaBr. Then, a NaClO solution (4 mmol g^{-1}) was added dropwise to catalyze the oxidation of primary alcohol groups, maintaining the pH at approximately 10.5. Once the pH stabilized, the reaction was terminated, and HCl was added to adjust the pH to 7. The solution was ultrasonicated at 600 W for 30 min to obtain the TOCNFs suspension. The prepared TOCNFs suspension was then mixed with CNTs at a 1:1 mass ratio. After stirring for 30 min, the mixture was ultrasonicated at 300 W for 1 h and subsequently processed using a high-speed centrifugal defoaming mixer to remove air bubbles. Finally, excess water was removed to obtain a conductive ink with a mass fraction of 4% CNT/TOCNFs.

3D Printing and programmable design of TWF electronics

The printing process used a bioprinter equipped with a pneumatic dispenser (ROKIT Healthcare, INC, South Korea). Specifically, the ink was put into a precision stainless steel syringe with a needle diameter of 1 mm, and centrifuged to remove the residual air in the syringe, and then the syringe was connected to an air control system for pressure adjustment. Printing speed was controlled by the Newcreator software of the 3D printer. The printed layers were patterned around 1 mm thick. The circuits were designed using 3D MAX 2019 software, which were then converted to G-code using Newcreator software for the further printing. Circuit patterns were printed on the TWF by running this G-code program.

Characterizations

The morphologies of the wood samples in cross-section and longitudinal direction were observed using a scanning electron microscope

(SEM, JSM-7600F, Japan Electron Optics Co., Ltd.) with an accelerating voltage of 15 kV. Composition analysis (cellulose, hemicellulose, and lignin) was determined according to the sulfuric acid hydrolysis method (NY/T 1459-2007 and GB/T 20805-2006). Mechanical tensile tests were performed using an INSTRON 5966 universal testing machine. The surface profile was measured using an atomic force microscope (AFM, Dimesion Edge, Germany) to assess roughness. Absorbance/transmission intensity was collected using a UV-Vis-NIR spectrophotometer (Shimadzu UV3600 plus, Japan) in a wavelength range of 200–800 nm. Fourier transform infrared spectroscopy (FTIR, VERTEX 80 V, Germany) was carried out in a wavelength range of 400–400 cm^{-1}. Fluorescent images were taken by a confocal fluorescent microscopy (Leica SP5 II, Germany). X-ray synchrotron scattering experiment was conducted in Australian Synchrotron (ANSTO, Clayton Australia) SAXS/WAXS beamline with a wavelength of $\lambda = 0.685$ Å and detector distance of 320 mm. Nitrogen physisorption was performed on a Micromeritics ASAP 2020HD88 instrument at 77 K. The output current of the sensor was analyzed by electrochemical workstation (CHI660E, China) with an input voltage of 2 V and an interval of 0.1 s. The thermal tolerance experiment was performed by a thermal infrared imaging camera (FOTRIC 600 C) between 25 °C to 115 °C at a relative humidity range of 65–95%. The details of finite element method simulation are provided in Supplementary Methods (Supplementary Information). The sheet resistance (R_s, in Ohm/sq) was measured using a four-probe tester and a thin-film linear four-probe probe four-probe (ST2258C, China) with the probes configured in a spacing of 2 mm. The calculation of the sheet resistance (R_s) for thin samples is based on the following equation[72]:

$$Rs = \frac{\pi}{ln2} \cdot \frac{E}{I} \cdot G \cdot D \cdot C \tag{1}$$

where I (A) and E (V) are the supplied current and measured voltage, respectively. The sheet resistance correlates to the correction factors related to the dimensions of the samples. The size of the measured sample is 3×55 mm^2 with a thickness of 30.9 ± 30 μm, the thickness correction coefficient G = 0.0111, the shape and position correction D = 0.3287, and the probe correction coefficient C = 1.256. The cyclic folding tests (90° to 180°) were performed using the Modular Flex Test System (Flex Test-X, China).

Data availability
The authors declare that the main data supporting the findings of this study are available within the article and its Supplementary Information. Extra data are available from the corresponding author upon request.

References
1. Ju, S. et al. Fabrication of fully transparent nanowire transistors for transparent and flexible electronics. *Nat. Nanotechnol.* **2**, 378–384 (2007).
2. Oh, J. Y. & Bao, Z. Second skin enabled by advanced electronics. *Adv. Sci.* **6**, 1900186 (2019).
3. Karnaushenko, D. et al. High-performance magnetic sensorics for printable and flexible electronics. *Adv. Mater.* **27**, 880–885 (2015).
4. Han, S. T. et al. An overview of the development of flexible sensors. *Adv. Mater.* **29**, 1700375 (2017).
5. Wang, T. et al. Flexible transparent electronic gas sensors. *Small* **12**, 3748–3756 (2016).
6. Lim, Y. W., Jin, J. & Bae, B. S. Optically transparent multiscale composite films for flexible and wearable electronics. *Adv. Mater.* **32**, 1907143 (2020).
7. Tan, Y. J. et al. A transparent, self-healing and high-κ dielectric for low-field-emission stretchable optoelectronics. *Nat. Mater.* **19**, 182–188 (2020).
8. Zhao, C., Liu, Y., Beirne, S., Razal, J. & Chen, J. Recent development of fabricating flexible micro-supercapacitors for wearable devices. *Adv. Mater. Technol.* **3**, 1800028 (2018).
9. Yan, Z., Luo, S., Li, Q., Wu, Z. S. & Liu, S. Recent advances in flexible wearable supercapacitors: properties, fabrication, and applications. *Adv. Sci.* **11**, 2302172 (2023).
10. Pierre Claver, U. & Zhao, G. Recent progress in flexible pressure sensors based electronic skin. *Adv. Eng. Mater.* **23**, 2001187 (2021).
11. Ma, L. et al. Full-textile wireless flexible humidity sensor for human physiological monitoring. *Adv. Funct. Mater.* **29**, 1904549 (2019).
12. Cheng, S. et al. Ultrathin hydrogel films toward breathable skin-integrated electronics. *Adv. Mater.* **35**, 2206793 (2023).
13. Makushko, P. et al. Flexible magnetoreceptor with tunable intrinsic logic for on-skin touchless human-machine interfaces. *Adv. Funct. Mater.* **31**, 2101089 (2021).
14. Dai, Y., Hu, H., Wang, M., Xu, J. & Wang, S. Stretchable transistors and functional circuits for human-integrated electronics. *Nat. Electron.* **4**, 17–29 (2021).
15. Hamedi, M. et al. Integrating electronics and microfluidics on paper. *Adv. Mater.* **28**, 5054 (2016).
16. Yamagishi, K. et al. Flexible and stretchable liquid-metal microfluidic electronics using directly printed 3D microchannel networks. *Adv. Funct. Mater.* **34**, 2311219 (2023).
17. Utz, M. & Landers, J. Magnetic resonance and microfluidics. *Science* **330**, 1056–1058 (2010).
18. Ju, H. et al. A locally actuatable soft robotic film for actively reconfiguring shapes of flexible electronics. *Soft Robot.* **9**, 767–775 (2022).
19. Kaltenbrunner, M. et al. An ultra-lightweight design for imperceptible plastic electronics. *Nature* **499**, 458–463 (2013).
20. Yaqing, L., Ke, H., Geng, C., Ru, L. W. & Xiaodong, C. Nature-inspired structural materials for flexible electronic devices. *Chem. Rev.* **117**, 12893 (2017).
21. Keplinger, T., Wittel, F. K., Rüggeberg, M. & Burgert, I. Wood derived cellulose scaffolds—processing and mechanics. *Adv. Mater.* **33**, 2001375 (2021).
22. De France, K., Zeng, Z., Wu, T. & Nyström, G. Functional materials from nanocellulose: utilizing structure–property relationships in bottom-up fabrication. *Adv. Mater.* **33**, 2000657 (2021).
23. Yue, X. et al. Tough and moldable sustainable cellulose-based structural materials via multiscale interface engineering. *Adv. Mater.* **36**, 2306451 (2024).
24. Liu, R. et al. Producing a room temperature phosphorescent film from natural wood using a top-down approach. *Adv. Funct. Mater.* **34**, 2312254 (2024).
25. Kumar, A., Jyske, T. & Petric, M. Delignified wood from understanding the hierarchically aligned cellulosic structures to creating novel functional materials: a review. *Adv. Sustain. Syst.* **5**, 2000251 (2021).
26. Zhang, T. et al. Flexible transparent sliced veneer for alternating current electroluminescent devices. *ACS Sustain. Chem. Eng.* **7**, 11464–11473 (2019).
27. Tang, Q., Fang, L., Wang, Y., Zou, M. & Guo, W. Anisotropic flexible transparent films from remaining wood microstructures for screen protection and AgNW conductive substrate. *Nanoscale* **10**, 4344–4353 (2018).
28. Zhang, T. et al. Constructing a novel electroluminescent device with high-temperature and high-humidity resistance based on a flexible transparent wood film. *ACS Appl. Mater. Interfaces* **11**, 36010–36019 (2019).
29. Fu, Q., Chen, Y. & Sorieul, M. Wood-based flexible electronics. *ACS Nano* **14**, 3528–3538 (2020).
30. Zhu, H. et al. Wood-derived materials for green electronics, biological devices, and energy applications. *Chem. Rev.* **116**, 9305–9374 (2016).

31. Jiang, F. et al. Wood-based nanotechnologies toward sustainability. *Adv. Mater.* **30**, 1703453 (2018).

32. Jung, Y. H. et al. High-performance green flexible electronics based on biodegradable cellulose nanofibril paper. *Nat. Commun.* **6**, 7170 (2015).

33. Dai, S. et al. Intrinsically ionic conductive cellulose nanopapers applied as all solid dielectrics for low voltage organic transistors. *Nat. Commun.* **9**, 2737 (2018).

34. Park, J. et al. Flexible and transparent organic phototransistors on biodegradable cellulose nanofibrillated fiber substrates. *Adv. Opt. Mater.* **6**, 1701140 (2018).

35. Kumar, A., Jyske, T. & Petric, M. Delignified wood from understanding the hierarchically aligned cellulosic structures to creating novel functional materials: a review. *Adv. Sustain. Syst.* **5**, 45 (2021).

36. Tran, V. C. et al. Electrical current modulation in wood electrochemical transistor. *Proc. Natl Acad. Sci. USA* **120**, e2218380120 (2023).

37. Jakob, M. et al. The strength and stiffness of oriented wood and cellulose-fibre materials: A review. *Prog. Mater. Sci.* **125**, 100916 (2022).

38. Han, X., Ye, Y., Lam, F., Pu, J. & Jiang, F. Hydrogen-bonding-induced assembly of aligned cellulose nanofibers into ultrastrong and tough bulk materials. *J. Mater. Chem. A* **7**, 27023–27031 (2019).

39. Liu, G., Zhao, Y., Wu, G. & Lu, J. Origami and 4D printing of elastomer-derived ceramic structures. *Sci. Adv.* **4**, eaat0641 (2018).

40. Overvelde, J. T., Weaver, J. C., Hoberman, C. & Bertoldi, K. Rational design of reconfigurable prismatic architected materials. *Nature* **541**, 347–352 (2017).

41. Rus, D. & Tolley, M. T. Design, fabrication and control of origami robots. *Nat. Rev. Mater.* **3**, 101–112 (2018).

42. Treml, B., Gillman, A., Buskohl, P. & Vaia, R. Origami mechanologic. *Proc. Natl Acad. Sci. USA* **115**, 6916–6921 (2018).

43. Chen, Y., Peng, R. & You, Z. Origami of thick panels. *Science* **349**, 396–400 (2015).

44. Yan, W. et al. Origami-based integration of robots that sense, decide, and respond. *Nat. Commun.* **14**, 1553 (2023).

45. Xu, Y. et al. Pencil–paper on-skin electronics. *Proc. Natl Acad. Sci. USA* **117**, 18292–18301 (2020).

46. Niu, G. et al. Pencil-on-paper humidity sensor treated with NaCl solution for health monitoring and skin characterization. *Nano Lett.* **23**, 1252–1260 (2023).

47. Li, S., Chu, J., Li, B., Chang, Y. & Pan, T. Handwriting iontronic pressure sensing Origami. *ACS Appl. Mater. Interfaces* **11**, 46157–46164 (2019).

48. Yan, J. et al. Direct-ink writing 3D printed energy storage devices: From material selectivity, design and optimization strategies to diverse applications. *Mater. Today* **54**, 110–152 (2022).

49. Liu, C. et al. 3D printing of customized lignocellulose nanofibril aerogels for efficient thermal insulation. *Addit. Manuf.* **78**, 103841 (2023).

50. Zhou, G., Li, M.-C., Liu, C., Wu, Q. & Mei, C. 3D Printed Ti3C2Tx MXene/Cellulose Nanofiber architectures for solid-state supercapacitors: ink rheology, 3D printability, and electrochemical performance. *Adv. Funct. Mater.* **32**, 2109593 (2022).

51. Na, J. H. et al. Programming reversibly self-folding origami with micropatterned photo-crosslinkable polymer trilayers. *Adv. Mater.* **27**, 79–85 (2015).

52. Ze, Q. et al. Spinning-enabled wireless amphibious origami millirobot. *Nat. Commun.* **13**, 3118 (2022).

53. Cheng, Y. C., Lu, H. C., Lee, X., Zeng, H. & Priimagi, A. Kirigami-based light-induced shape-morphing and locomotion. *Adv. Mater.* **32**, 1906233 (2020).

54. Fu, Q., Ansari, F., Zhou, Q. & Berglund, L. A. Wood nanotechnology for strong, mesoporous, and hydrophobic biocomposites for selective separation of oil/water mixtures. *ACS Nano* **12**, 2222–2230 (2018).

55. Zhu, S. et al. Transparent wood-based functional materials via a top-down approach. *Prog. Mater. Sci.* **132**, 101025 (2023).

56. Wang, C. et al. Fabrication of robust paper-based electronics by adapting conventional paper making and coupling with wet laser writing. *ACS Sustain. Chem. Eng.* **11**, 9782 (2023).

57. Yang, X., Shi, K., Zhitomirsky, I. & Cranston, E. D. Cellulose nanocrystal aerogels as universal 3D lightweight substrates for supercapacitor materials. *Adv. Mater.* **27**, 6104–6109 (2015).

58. Zhou, G. et al. 3D printed nitrogen-doped thick carbon architectures for supercapacitor: ink rheology and electrochemical performance. *Adv. Sci.* **10**, 2206320 (2023).

59. Yang, X. & Berglund, L. A. Structural and ecofriendly holocellulose materials from wood: microscale fibers and nanoscale fibrils. *Adv. Mater.* **33**, 2001118 (2021).

60. Mietner, J. B., Jiang, X., Edlund, U., Saake, B. & Navarro, J. R. 3D printing of a bio-based ink made of cross-linked cellulose nanofibrils with various metal cations. *Sci. Rep.* **11**, 6461 (2021).

61. Li, K. et al. Self-densification of highly mesoporous wood structure into a strong and transparent film. *Adv. Mater.* **32**, 2003653 (2020).

62. Wang, Y. et al. Organic crystalline materials in flexible electronics. *Chem. Soc. Rev.* **48**, 1492–1530 (2019).

63. Hajian, A., Wang, Z., Berglund, L. A. & Hamedi, M. M. Cellulose nanopaper with monolithically integrated conductive micropatterns. *Adv. Electron. Mater.* **5**, 1800924 (2019).

64. Biswas, S. K. et al. Thermally superstable cellulosic-nanorod-reinforced transparent substrates featuring microscale surface patterns. *ACS Nano* **13**, 2015–2023 (2019).

65. Apostolopoulou-Kalkavoura, V., Gordeyeva, K., Lavoine, N. & Bergström, L. Thermal conductivity of hygroscopic foams based on cellulose nanofibrils and a nonionic polyoxamer. *Cellulose* **25**, 1117–1126 (2018).

66. Chen, S., Chen, J., Zhang, X., Li, Z.-Y. & Li, J. Kirigami/origami: unfolding the new regime of advanced 3D microfabrication/nanofabrication with "folding. *Light Sci. Appl.* **9**, 75 (2020).

67. Yi, S. et al. High-throughput fabrication of soft magneto-origami machines. *Nat. Commun.* **13**, 4177 (2022).

68. Liu, Y., Shaw, B., Dickey, M. D. & Genzer, J. Sequential self-folding of polymer sheets. *Sci. Adv.* **3**, e1602417 (2017).

69. Silverberg, J. L. et al. Origami structures with a critical transition to bistability arising from hidden degrees of freedom. *Nat. Mater.* **14**, 389–393 (2015).

70. Al-Mulla, T. & Buehler, M. J. Folding creases through bending. *Nat. Mater.* **14**, 366–368 (2015).

71. Zheng, K. et al. Modularized paper actuator based on shape memory alloy, printed heater, and Origami. *Adv. Intell. Syst.* **4**, 2200194 (2022).

72. Miccoli, I., Edler, F., Pfnür, H. & Tegenkamp, C. The 100th anniversary of the four-point probe technique: the role of probe geometries in isotropic and anisotropic systems. *J. Phys. Condens. Matter* **27**, 223201 (2015).

Acknowledgements

Additional information
Supplementary information The online version contains supplementary material available at https://doi.org/10.1038/s41467-024-53708-1.

Correspondence and requests for materials should be addressed to Yanjun Xie or Qiliang Fu.

Peer review information *Nature Communications* thanks Ankur Mehta, and the other, anonymous, reviewers for their contribution to the peer review of this work. A peer review file is available.

Reprints and permissions information is available at http://www.nature.com/reprints

Publisher's note Springer Nature remains neutral with regard to jurisdictional claims in published maps and institutional affiliations.